



Published in final edited form as:

Geophys Res Lett. 2019 January 28; 46(2): 1049–1060. doi:10.1029/2018GL081095.

High resolution mapping of nitrogen dioxide with TROPOMI: First results and validation over the Canadian oil sands

Debora Griffin¹, Chris A. McLinden¹, Folkert Boersma^{2,3}, Adam Bourassa⁴, Enrico Dammers¹, Doug Degenstein⁴, Henk Eskes², Lukas Fehr⁴, Vitali Fioletov¹, Katherine Hayden¹, Shailesh K. Kharol¹, Shao-Meng Li¹, Paul Makar¹, Randall V. Martin⁵, Cristian Mihele¹, Richard L. Mittermeier¹, Nickolay Krotkov⁶, Maarten Sneep², Lok N. Lamsal^{6,7}, Mark ter Linden^{2,8}, Jos van Geffen², Pepijn Veefkind^{2,9}, Mengistu Wolde¹⁰, Xiaoyi Zhao¹

¹Air Quality Research Division, Environment and Climate Change Canada, Toronto, Ontario, Canada ²Royal Netherlands Meteorological Institute (KNMI), De Bilt, The Netherlands ³Wageningen University, Environmental Sciences Group, Wageningen, The Netherlands ⁴Institute of Space and Atmospheric Studies, University of Saskatchewan, Saskatoon, Saskatchewan, Canada ⁵Dalhousie University, Department of Physics and Atmospheric Science, Halifax, Nova Scotia, Canada ⁶Laboratory for atmospheric chemistry and dynamics, NASA Goddard Space Flight Center, Greenbelt, MD, USA ⁷Goddard Earth Sciences Technology and Research, Universities Space Research Association, Columbia, MD, USA ⁸Science and Technology (S&T), Delft, Netherlands ⁹Delft University of Technology, Delft, The Netherlands ¹⁰National Research Council Canada, Flight Research Laboratory, Ottawa, K1A 0R6, Canada

Abstract

TROPOMI, on-board the Sentinel-5 Precursor satellite is a nadir-viewing spectrometer measuring reflected sunlight in the ultraviolet, visible, near-infrared, and shortwave infrared spectral range. From these spectra several important air quality and climate-related atmospheric constituents are retrieved at an unprecedented high spatial resolution, including nitrogen dioxide (NO₂). We present the first retrievals of TROPOMI NO₂ over the Canadian Oil Sands, contrasting them with observations from the OMI satellite instrument, and demonstrate its ability to resolve individual plumes and highlight its potential for deriving emissions from individual mining facilities. Further, the first TROPOMI NO₂ validation is presented, consisting of aircraft and surface in-situ NO₂ observations, as well as ground-based remote-sensing measurements between March and May 2018. Our comparisons show that the TROPOMI NO₂ vertical column densities are highly correlated with the aircraft and surface in-situ NO₂ observations, and the ground-based remote-sensing measurements with a low bias (15–30 %) over the Canadian Oil Sands.

Plain Language Summary—Nitrogen dioxide (NO₂) is a pollutant that is linked to respiratory health issues and has negative environmental impacts such as soil and water acidification. Near the surface the most significant sources of NO₂ are fossil fuel combustion and biomass burning. With a recently launched satellite instrument (TROPOspheric Monitoring Instrument; TROPOMI) NO₂ can be measured with an unprecedented combination of accuracy, spatial coverage, and resolution.

This work presents the first TROPOMI NO₂ measurements near the Canadian Oil Sands and shows that these measurements have an outstanding ability to detect NO₂ on a very high horizontal resolution that is unprecedented for satellite NO₂ observations. Further, these satellite measurements are in excellent agreement with aircraft and ground-based measurements.

1 Introduction

The ability to observe the near-surface abundance of air pollutants from space has drastically increased over the last two decades. The first space-borne ultraviolet-visible spectrometer focusing on tropospheric trace composition was the Global Ozone Monitoring Experiment (GOME), 1995–2011, with a pixel size of $40 \times 320 \text{ km}^2$ [Burrows et al., 1999], followed by the SCanning Imaging Absorption spectroMeter for Atmospheric Cartography (SCIAMACHY), 2002–2012 ($30 \times 60 \text{ km}^2$) [Bovensmann et al., 1999] and the GOME-2 instruments (2006–present, 2012–present; $40 \times 80 \text{ km}^2$) [Callies et al., 2000]. Until now, the previous standard was the Ozone Monitoring Instrument (OMI; 2004–present; $13 \times 24 \text{ km}^2$) [Levelt et al., 2006; Krotkov et al., 2016], that was able to resolve pollutant distributions at the urban scale (20–30 km), from which emissions could be inferred for large point sources [e.g. Lu and Streets, 2012; Ghude et al., 2013; de Foy et al., 2015]. However, with the launch of the European Space Agency's (ESA) Sentinel-5 Precursor (S-5P) on October 13, 2017, space-borne measurements have entered a new era. In addition to spatial resolution, data product quality of the recorded spectra has significantly increased for this type of space-borne UV-vis spectrometer over the past two decades.

Here, we focus on the first retrieval results of tropospheric NO₂ from TROPOMI. NO₂ is an important pollutant gas that is linked to respiratory health issues [Health Canada, 2018] and has negative environmental impacts such as soil and water acidification [Environment Canada, 2018]. NO₂ is emitted mainly as nitrogen monoxide (NO) by combustion processes, such as fossil fuel combustion and biomass burning, as well as lightning, where molecular nitrogen (N₂) combines with molecular oxygen (O₂) at extremely high temperatures. Due to the rapid cycling between them, NO and NO₂ are often considered together as NO_x (NO + NO₂). Within a plume, the lifetime of NO_x is relatively short, on the order of a few hours, and is in daytime primarily removed by reaction with the hydroxyl radical (OH). Due to this short lifetime, background NO₂ concentrations can be orders of magnitude smaller than levels over polluted areas.

This study presents the first TROPOMI tropospheric NO₂ retrievals (offline v.101) [van Geffen et al., 2018; Boersma et al., 2018] and demonstrates its ability to resolve individual plumes from space at an unprecedented spatial resolution. To demonstrate the quality of the TROPOMI NO₂ product and its suitability for high-resolution mapping, aircraft and ground-based data over the Athabasca Oil Sands Region (AOSR) in north-eastern Alberta, Canada are used for its evaluation. The AOSR, and in particular the surface mining area at 57°N, is a remote area that has significant NO_x emissions from a variety of types of industrial sources, such as upgraders (a facility that converts bitumen, a viscous form of oil found in the oil sands, into synthetic crude oil) and heavy transportation vehicles [McLinden et al., 2012; Percy et al., 2012]. As such, this region is an ideal location for evaluating the TROPOMI NO₂ retrieval product and its ability to capture localized enhancements of NO₂,

including individual plumes, and low background values over a relatively small domain. We also contrast these results with a similar analysis of lower resolution OMI observations to help demonstrate the importance of the finer spatial resolution in capturing horizontal gradients and small scale features.

The measurements shown here were taken between March and May, 2018 and for much of this period the surface was snow-covered (note that data for March is pre-operational and may be slightly noisier). In principle, this highly reflective surface enables a more accurate retrieval with larger signals and less dependence on the knowledge of profile shape [e.g., *O'Byrne et al.*, 2010; *McLinden et al.*, 2014]. Current retrieval algorithms can struggle due to the requirement for identifying the presence of snow and also correctly accounting for its altered reflectance properties. The surface mines of the AOSR are also surrounded by boreal forest that is associated with a very low reflectance, providing the additional challenge of a changing albedo over a small area.

2 Datasets

2.1 Satellite NO₂ data

TROPOMI is the single payload on the S-5P satellite that has a Sun-synchronous orbit with a local overpass time of around 1:30pm and has near full-surface coverage on a daily basis [*Veefkind et al.*, 2012; *Hu et al.*, 2018]. The instrument contains four spectrometers, three that cover the Ultra-Violet-Near Infra-Red (UV-NIR) with two spectral bands at 270–500nm and 675–775nm, and one for the SWIR. The TROPOMI NO₂ retrieval algorithm was developed by the Royal Netherlands Meteorological Institute (KNMI) and utilizes the bands of the UV-NIR spectrometer. The retrieval algorithm is based on the NO₂ DOMINO retrieval previously used for OMI spectra [*Boersma et al.*, 2011] with improvements made for all retrieval sub-steps [*van Geffen et al.*, 2015; *Lorente et al.*, 2017; *Zara et al.*, 2018] within the QA4ECV project [*Boersma et al.*, 2018; *van Geffen et al.*, 2018]. A tropospheric vertical column density (VCD, or simply ‘column’) is provided by the algorithm, which represents the vertically integrated number of NO₂ molecules per unit area between the surface and the tropopause (in units of mol/m², with typical columns ranging from 10–200 μmol/m²). To determine the crucial air mass factor (AMF), a measure of the measurement’s sensitivity [e.g. *Palmer et al.*, 2001; *McLinden et al.*, 2014], the profile shape of the TM5-MP model is used (at 1 × 1° resolution) *Williams et al.* [2017], the surface albedo information is derived from a monthly OMI climatology (on a 0.5 × 0.5° resolution) [*Kleipool et al.*, 2008]. TROPOMI uses a snow flag from the Near-real-time Ice and Snow Extent (NISE), and the albedo is set to 0.6 (over the AOSR) if the surface beneath is covered in snow or ice. For this study we use v1.01 [*van Geffen et al.*, 2018], the first released offline version of the TROPOMI tropospheric NO₂ columns (<https://s5phub.copernicus.eu>; <http://www.tropomi.eu>). Spatial resolution varies with across-track position and in this study the average pixel size is 6 × 7km. Pixels that are fully or partially covered by clouds were filtered, here we used 0.3 as a cut-off for the radiative cloud fraction (“cloud_fraction_crb_nitrogen_dioxide_window”).

OMI NO₂ observations (NASA Standard Product, SP, version 3.1; *Krotkov et al.* [2017]; *Marchenko et al.* [2015]) are used in order to evaluate the relative performance of

TROPOMI and OMI. The OMI data are filtered in a similar manner as TROPOMI with an additional restriction that only smaller pixels are considered (track positions 11–50), which are automatically removed in the SPv3.1 product.

2.2 In-situ measurements

Aircraft-borne in situ measurements were taken in April 2018 over the AOSR as part of Environment and Climate Change Canada's (ECCC's) aircraft campaign. Here, we use measurements taken during three flights, on April 5, 9, and 13, 2018 between 16:30UTC and 21:00UTC. The TROPOMI overpasses in this region are typically between 19:00 UTC and 21:00 UTC; on some days two overpasses occur that are approximately 100 min apart. During those flights, air parcels were sampled in the planetary boundary layer (PBL) between approximately 200 to 400 m agl (above ground level) with occasional spiral flights reaching up to 2300 m agl.

The aircraft in-situ NO₂ measurements were taken on-board a National Research Council of Canada's Convair 580 research aircraft using two Thermo Scientific Model 42i-TL (NO-NO₂-NO_x) Analyzers, modified to measure at 1Hz time resolution. The first analyzer measured NO directly, while the second analyzer measured the sum of NO and large fraction of NO₂ (65 %), selectively converted to NO using a photolytic converter (Air Quality Design Inc.). NO₂ was then calculated by difference and averaged to 3s, with an estimated detection limit of 0.2 ppbv.

Ground-based NO₂ in-situ concentrations are continuously sampled at 17 locations in north-eastern Alberta as part of the Wood Buffalo Environment Association (WBEA; <http://wbea.org/historical-monitoring-data/>) [Percy *et al.*, 2012]. NO₂ concentrations (measured in a similar way as described above for the aircraft measurements, see supplementary material) are available every 5 min.

2.3 Pandora instrument

A type of ground-based spectrometer, known as Pandora, has been developed to help evaluate satellite NO₂ retrievals [Herman *et al.*, 2009]. The Pandora instrument measures direct sunlight in the UV-vis spectral range (280–525 nm). High-quality NO₂ total columns (tropospheric + stratospheric) are obtained by using the differential optical absorption spectroscopy (DOAS) technique [Noxon, 1975; Platt and Stutz, 2008] in 400 to 440 nm range. The retrieved NO₂ total columns data has a precision of $\pm 2.7 \times 10^{14}$ molec/cm² [Herman *et al.*, 2009]. A Pandora instrument has been deployed in Fort McKay in the AOSR (57.184°N, 111.64°W) since 2013 [Fioletov *et al.*, 2016]. NO₂ columns are available approximately every 1.5 min under unobscured Sun conditions.

2.4 Alternative AMF

We also re-calculate the AMFs and examine their impact on the TROPOMI tropospheric NO₂ columns over the AOSR. The procedure is similar to that from McLinden *et al.* [2014] with the following differences: (1) GEM-MACH version 2, at 10 km resolution, updated emissions and using output at the time of the satellite overpass was used to provide the NO₂ profile shape; (2) Interactive Multisensor Snow and Ice Mapping System (IMS) [Helfrich *et*

al., 2007] at 4 km resolution was used to flag pixels with snow-cover; and the use of the SASKTRAN radiative transfer model [Bourassa et al., 2008; Zawada et al., 2015; Dueck et al., 2017] for the generation of the AMF look-up tables. SASKTRAN is employed here as it is more readily able to implement future planned improvements such as non-Lambertian surfaces. The cloud input needed for the estimation is taken from the TROPOMI product (“cloud_fraction_crb_nitrogen_dioxide_window”, “cloud_fraction_crb_nitrogen_dioxide_window”, “cloud_pressure_crb”).

An uncertainty is estimated for the alternative tropospheric columns (similar to *McLinden et al.* [2014]) by adding the uncertainty of the slant column density (provided in the S5P NO₂ data product), the uncertainty of the stratospheric column density (provided in the S5P NO₂ data product), and the uncertainty of the alternative AMF (assumed to be 20 %) in quadrature. The uncertainty of the AMF contains uncertainties from cloud fraction, cloud pressure, albedo, surface pressure and profile shape [*McLinden et al.*, 2014].

3 TROPOMI over the Canadian oil sands

Before the launch of TROPOMI, OMI has been used extensively to study the distribution and evolution of NO₂ over the Canadian oil sands *McLinden et al.* [2012, 2016]. However, due to the small spatial extent of the surface mining, which is commensurate with OMI’s pixel size, it was not possible to observe individual plumes. It was only possible to reliably map the average distribution by considering several years together, and emissions estimates were for the mining region as a whole [*Fioletov et al.*, 2016].

Figure 1 a and b shows TROPOMI and OMI observations for a single day, April 9, 2018, over the AOSR surface mines. TROPOMI shows well defined plumes of significantly elevated NO₂ originating from two distinct mining areas from which it should be possible to estimate NO_x emissions. From the spatial location of the plumes in Fig. 1 a, it appears that the well-defined NO₂ plume in the south originates from the bitumen upgrading stacks which are elevated sources, while the more diffuse enhancement in the north is consistent with the heavy hauler trucks, a surface source. OMI, by contrast shows much more modest enhancements for about a half-dozen pixels and captures none of the fine details making its spatial distribution impossible to interpret. Averaging TROPOMI over the three month period of interest using the oversampling technique of *Fioletov et al.* [2011] provides a distribution very similar to that of an OMI multi-year average, but with much better resolved spatial patterns and higher peak values (Fig. 1 c and d). The distribution shows a separation of the NO₂ between the northern and southern mines.

4 Evaluation of the NO₂ product

4.1 Spiral flights

As noted in Sect. 2.2, spirals were flown (within ± 2 h of the TROPOMI overpass time) as high as 2300 m agl that penetrated the plume top. These types of aircraft measurements can be used to estimate the NO₂ VCDs in the PBL, as well as determine AMFs based on the measured NO₂ profiles. Using this true profile to calculate AMFs helps to identify errors in the retrieval, and further allows a more quantitative evaluation of AMFs derived using model

inputs. The aircraft profile spirals began as low as approximately 200 m agl, measuring volume mixing ratios (VMRs) throughout the PBL. To compare these to TROPOMI, we estimated a tropospheric NO₂ VCD using the aircraft measurements from those spirals. For this estimation, the aircraft measurements are binned into 100 m levels; between the surface and lowest aircraft altitude, we assume a well mixed layer and use the concentration of the lowest measurements. Above the maximum flight altitude we use NO₂ VMRs from the GEOS-Chem model accounting for $\sim 1.8 \times 10^{14}$ molec/cm². Temperatures and pressures needed for the calculation were taken from the operational GEM-MACH model. During the three aircraft flights, seven spirals were flown. Figure 2a shows the in-situ measurements of some spiral flights along with the GEM-MACH NO₂ VMRs (for the nearest grid-box at the closest hour). GEM-MACH reproduces the actual NO₂ measurements very well in the PBL and Fig. 2 shows that the profile is captured well by the model. However, it does not always capture the height of the boundary layer and, as such, there is disagreement above approximately 1.5km, where NO₂ VMRs drop to near zero in the model.

The comparison with the aircraft spirals indicates a low bias for TROPOMI (approximately -18 % compared to the aircraft measurements). This bias nearly disappears (<5 %) if the alternative AMFs are applied (panel c). Figure 2d shows the “true” AMF estimated using the albedo as used in the TROPOMI input file (orange), and using the MODIS albedo (red). The comparison (Fig. 2d) shows that the AMFs (using the MODIS albedo) from the aircraft measurements are very close to the estimated AMFs (blue) using the GEM-MACH model, and that TROPOMI tropospheric AMFs (green) are likely overestimated in this region (above snow). It also shows that a wrong profile shape over the AOSR and an albedo that is too high can cancel each other’s effects, leading to a TROPOMI AMF value close to the “true” AMF (red). This highlights the benefits of using of a high-resolution regional model which reproduces AMFs close to the true/measured AMFs.

4.2 Spatial correlation with the aircraft measurements

While tropospheric NO₂ VCDs can be estimated from the spirals, only seven are available for comparison with TROPOMI NO₂ VCDs. In this section, we evaluate the ability of TROPOMI to detect localized enhancements of tropospheric NO₂ on the scale of its pixel size, using all pixels and aircraft measurements to evaluate the ability of TROPOMI to capture spatial gradients. We average the all aircraft in-situ measurements of NO₂ for the three flights that are sampled below 1 km agl (to ensure the data collected is in the PBL), taken within ± 2 h within the overpass time, and that are within the area of the individual TROPOMI pixel. For all three flights the surface below was covered completely in snow and ice (Fig. S2). On average, over 150 aircraft in-situ NO₂ measurements with an integration time of 3s were taken within one TROPOMI pixel, and some pixels contain as many as 700. The aircraft in-situ and the TROPOMI measurements (Fig. 3) correlate well, with a correlation coefficient $R \approx 0.7$, showing that TROPOMI captured the gradients and localized enhancements of NO₂ on it’s small pixel size of approximately 6×7 km. To be able to quantitatively compare the satellite VCDs to the in-situ VMRs, we convert the average in-situ measurements (at the average aircraft altitude, h , below 1000 m agl) into tropospheric VCDs using the daily output from the GEM-MACH model:

$$\text{VCD}_{\text{aircraft}} = \frac{C_{\text{aircraft}}(h)}{C_{\text{GEM-MACH}}(h)} \times \text{VCD}_{\text{GEM-MACH, PBL}} + \text{VCD}_{\text{GEOS-Chem, freetrop}}$$

The results (Fig.3 c) indicate a low bias of approximately 15 % for the TROPOMI tropospheric NO₂ VCDs compared to the aircraft measurements, with a mean difference of -5.3×10^{14} molec/cm² (-21 %; TROPOMI-aircraft) and a random error of approximately 0.97×10^{15} molec/cm². After applying the correction to the TROPOMI VCDs (as described in Sect.2.4) the bias is reduced to 4 %, leading to an accuracy of -3.3×10^{14} molec/cm² (-13 %; TROPOMI-aircraft), and a random error of 1.27×10^{15} molec/cm². The improved slope in Fig. 3 d is expected given that the same profile shape is now used for both the scaling of aircraft concentrations and in the calculations of AMFs. The correlation between the aircraft measurements and the TROPOMI retrievals does not change using the alternative AMFs.

4.3 Comparison with ground-based measurements

To evaluate TROPOMI's ability to capture NO₂ distributions over a longer time and spatial scale than that covered by the aircraft flights, comparisons are made with measurements from a ground-based in-situ network (WBEA). This allows for a longer time period and larger area as for the aircraft data, discussed in the previous section. The results are displayed in Fig. 4a for measurements between March and May 2018, comparing the TROPOMI measurements from individual pixels to the averaged WBEA NO₂ measurements (± 30 min of the TROPOMI overpass). Only the TROPOMI pixels that cover the stations are used (due to the small size of the TROPOMI pixel and the distance between the WBEA stations, one pixel only covers one station). Overall, there is a good correlation between the TROPOMI tropospheric VCDs and the surface measurements ($R = 0.65$). To examine the theoretical correlation with surface measurements, we utilize output from an offline run of GEM-MACH at 2.5 km resolution. The correlation between model VCD and model surface VMR without any noise is roughly 0.6 (Fig. S5) and only decreases slightly with increased smoothing. Considering the observed correlation, with measurement noise, is comparable to this or slightly higher than that from these noise-free simulations, it appears that the reduction in correlation from unity is mainly due to the mismatch in the qualities being compared (column vs. surface) and little from the noise in either type of observation.

For the comparison with the TROPOMI NO₂ tropospheric columns, we average the Pandora data (± 30 min of the TROPOMI overpass) and subtract the corresponding TROPOMI NO₂ stratospheric columns to obtain a tropospheric Pandora columns. A good agreement was found between the TROPOMI and the Pandora columns (Fig. 4b). The theoretical correlation is expected around 0.95 with a slope of 0.85–0.9 at TROPOMI resolution (Fig. S5). The regression analysis shows a low bias for the TROPOMI tropospheric NO₂ VCDs with a slope of approximately 0.7. The slope increases to 0.75 when the alternative AMF is applied, which is only 0.1 lower than the expected slope (Fig. 4c); the correlation, however, slightly decreases.

While most of the ground in March and April was covered by snow, there are snow-free days at the end of April and in May over the AOSR. However, even for the snow-free days a small

low bias of the original TROPOMI NO₂ VCDs remains over the AOSR. Also for snow-free days, we found that the MODIS albedo is approximately half of the climatological OMI albedo used as input for the original AMFs (Fig. S4). This low albedo appears to offset the effect of the TM5 model at 1° resolution which has the effect of diluting emissions and leading to profiles that are not sufficiently weighted to near-surface NO₂. The alternative and original TROPOMI NO₂ VCDs agree within the estimated uncertainties, however, the uncertainties associated with the original NO₂ tropospheric columns, which can be close to 100 % over snow, can be much reduced by higher-resolution input (Fig. S6).

5 Discussion and Conclusions

This study presents the first results of TROPOMI NO₂ VCDs over the AOSR. We found that TROPOMI has an outstanding ability to detect tropospheric NO₂ on a very high horizontal resolution. The noise of the individual TROPOMI pixels is quite low, and without averaging there is a high correlation ($\sim 0.8 - 0.7$) between the TROPOMI observations and the aircraft in-situ measurements in the boundary layer that sampled air across the TROPOMI pixels. As promised, the TROPOMI tropospheric NO₂ product can retrieve good quality information on a 6×7 km (and even smaller) pixel size that is unprecedented for satellite-remote sensing observations.

Further, TROPOMI displays a high correlation with ground-based in-situ and remote sensing measurements that is unprecedented for satellite-remote sensing measurements of NO₂. Its predecessor, OMI (NO₂ SPv3.1), only shows low to moderate correlation with ground-based in-situ ($R = 0.35$) and remote-sensing ($R = 0.06$) measurements if the same method is applied (supplementary material). For the ground-based in-situ and remote-sensing measurements, there is a good correlation ($R \approx 0.68$) with TROPOMI NO₂. Again, this is a significant improvement to previous satellite and ground-based in-situ comparisons where measurements are typically averaged over years to achieve a good correlation [McLinden *et al.*, 2014] or the correlation is moderate ($R \approx 0.4$) if no corrections are applied [Kramer *et al.*, 2008].

Quantitatively we found a low bias of -15 to -30 % of the TROPOMI tropospheric NO₂ columns over the AOSR that was consistent for all of the comparisons carried out in this study. Previously similar discrepancies have been identified for OMI, which were associated with issues of input data used to estimate the tropospheric AMF [McLinden *et al.*, 2014]. Here, we re-calculated the AMFs using higher resolution input data. This includes, a high-resolution model, GEM-MACH (10×10 km resolution), to estimate the NO₂ profile shape for the lower part of the troposphere, a better identification of snow-covered surfaces (IMS, on 4×4 km resolution) and the surface reflectivity from the MODIS satellite. This improved input data provided more precise information on surface cover and more appropriate albedo, if snow is present. Using the alternative tropospheric NO₂ VCDs, the low bias is reduced to between 0 and -25 %. Thus, the low bias is not due to the retrieval itself, but is associated with the input data used for the tropospheric AMF calculation. A low bias can be seen for both, snow-covered and snow-free surfaces, indicating that the issue is due to both, an incorrect albedo over snow and an inaccurate NO₂ profile shape over the AOSR. While using high-resolution input improves the tropospheric AMF and as such the tropospheric

NO₂ VCDs, this correction is not as significant as previously seen for OMI [McLinden *et al.*, 2014]. For differences where the recalculated NO₂ columns increased by a factor of two compared to the original, we only see a 5 – 15 % improvement of the bias when the alternative AMFs were used. We found that the TROPOMI tropospheric NO₂ v1.01 is well within the requirements of 25–50 % bias. Based on our analysis, we recommend to improve the albedo (particularly over snow), as well as the snow flag information for the global product. Secondly, regional products could be developed, using high-resolution model information to improve the NO₂ a priori. Furthermore, we conclude that the TROPOMI stratospheric NO₂ column estimates work well.

Overall, we found that the data quality, noise level and resolution of these satellite-borne NO₂ VCDs is unprecedented. These high-resolution TROPOMI NO₂ observations can allow to pin-point even kilometer-scale emission sources and estimate localized emissions from industry, cities or fires on a monthly and likely daily basis.

Supplementary Material

Refer to Web version on PubMed Central for supplementary material.

Acknowledgments

The authors would like to thank the Wood Buffalo Environmental Association (WBEA) for the provision of their in situ data. The Sentinel 5 Precursor TROPOMI Level 2 product is developed with funding from the Netherlands Space Office (NSO) and processed with funding from the European Space Agency (ESA). We acknowledge the NASA Earth Science Division for funding of OMI NO₂ product development and analysis, and the Air Quality Research Division support teams and the National Research Council aircraft pilots and technical support team for the aircraft measurement campaign. These measurements were carried out as part of the Oil Sands 2018 aircraft measurement campaign project, funded by the Oil Sands Monitoring (OSM) program by the Governments of Alberta and Canada.

References

- Boersma KF, Eskes HJ, Dirksen RJ, van der A RJ, Veefkind JP, Stammes P, Huijnen V, Kleipool QL, Sneep M, Claas J, Leitão J, Richter A, Zhou Y, and Brunner D. (2011), An improved tropospheric NO₂ column retrieval algorithm for the Ozone Monitoring Instrument, *Atmos. Meas. Tech.*, 4, 1905.
- Boersma KF, Eskes HJ, Richter A, De Smedt I, Lorente A, Beirle S, van Geffen JHGM, Zara M, Peters E, Van Roozendaal M, Wagner T, Maasakkers JD, van der A J, Nightingale J, De Rudder A, Irie H, Pinardi G, Lambert J-C, and Compernelle (2018), Improving algorithms and uncertainty estimates for satellite NO₂ retrievals: Results from the Quality Assurance for Essential Climate Variables (QA4ECV) project, *Atmospheric Measurement Techniques Discussions*, 2018, 1–70, doi: 10.5194/amt-2018-200.
- Bourassa A, Degenstein D, and Llewellyn E. (2008), SASKTRAN: A spherical geometry radiative transfer code for efficient estimation of limb scattered sunlight, *Journal of Quantitative Spectroscopy and Radiative Transfer*, 109(1), 52 – 73, doi: 10.1016/j.jqsrt.2007.07.007.
- Bovensmann H, Burrows JP, Buchwitz M, Frerick J, Noël S, Rozanov VV, Chance KV, and Goede APH (1999), SCIAMACHY: Mission Objectives and Measurement Modes, *Journal of the Atmospheric Sciences*, 56(2), 127–150, doi:10.1175/1520-0469(1999)056<0127:SMOAMM>2.0.CO;2.
- Burrows JP, Weber M, Buchwitz M, Rozanov V, Ladstätter-Weißmayer A, Richter A, DeBeek R, Hoogen R, Bramstedt K, Eichmann K-U, Eisinger M, and Perner D. (1999), The Global Ozone Monitoring Experiment (GOME): Mission Concept and First Scientific Results, *Journal of the Atmospheric Sciences*, 56(2), 151–175, doi:10.1175/1520-0469(1999)056<0151:TGOMEG>2.0.CO;2.

- Callies J, Corpaccioli E, Eisinger M, Hahne A, and Lefebvre A. (2000), GOME-2-Metop's second-generation sensor for operational ozone monitoring, 102, 28–36.
- de Foy B, Lu Z, Streets DG, Lamsal LN, and Duncan BN (2015), Estimates of power plant NO_x emissions and lifetimes from OMI NO₂ satellite retrievals, *Atmospheric Environment*, 116, 1 – 11, doi:10.1016/j.atmosenv.2015.05.056.
- Dueck SR, Bourassa AE, and Degenstein DA (2017), An efficient algorithm for polarization in the SASKTRAN radiative transfer framework, *Journal of Quantitative Spectroscopy and Radiative Transfer*, 199, 1 – 11, doi: 10.1016/j.jqsrt.2017.05.016.
- Environment Canada (2018), Air pollution: drivers and impacts, <http://www.ec.gc.ca/indicateurs-indicateurs/default.asp?lang=En&n=D189C09D-1>; last accessed: 24 September 2018.
- Fioletov VE, McLinden CA, Krotkov N, Moran MD, and Yang K. (2011), Estimation of SO₂ emissions using OMI retrievals, *Geophysical Research Letters*, 38(21), doi:10.1029/2011GL049402.
- Fioletov VE, McLinden CA, Cede A, Davies J, Mihele C, Natcheva S, Li S-M, and O'Brien J. (2016), Sulfur dioxide (SO₂) vertical column density measurements by Pandora spectrometer over the Canadian oil sands, *Atmospheric Measurement Techniques*, 9(7), 2961–2976, doi:10.5194/amt-9-2961-2016.
- Ghude SD, Kulkarni SH, Jena C, Pfister GG, Beig G, Fadnavis S, and van der A RJ (2013), Application of satellite observations for identifying regions of dominant sources of nitrogen oxides over the Indian Subcontinent, *Journal of Geophysical Research: Atmospheres*, 118(2), 1075–1089, doi:10.1029/2012JD017811.
- Health Canada (2018), Human Health Risk Assessment for Ambient Nitrogen Dioxide, <https://www.canada.ca/en/health-canada/services/publications/healthy-living/human-health-risk-assessment-ambient-nitrogen-dioxide.html>; last accessed: 24 September 2018.
- Helfrich SR, McNamara D, Ramsay BH, Baldwin T, and Kasheta T. (2007), Enhancements to, and forthcoming developments in the Interactive Multisensor Snow and Ice Mapping System (IMS), *Hydrological Processes*, 21(12), 1576–1586, doi: 10.1002/hyp.6720.
- Herman J, Cede A, Spinei E, Mount G, Tzortziou M, and Abuhassan N. (2009), NO₂ column amounts from ground-based Pandora and MFDOAS spectrometers using the direct-sun DOAS technique: Intercomparisons and application to OMI validation, *Journal of Geophysical Research: Atmospheres*, 114(D13), doi:10.1029/2009JD011848.
- Hu H, Landgraf J, Detmers R, Borsdorff T, de Brugh JA, Aben I, Butz A, and Hasekamp O. (2018), Toward Global Mapping of Methane With TROPOMI: First Results and Intersatellite Comparison to GOSAT, *Geophysical Research Letters*, 45(8), 3682–3689, doi:10.1002/2018GL077259.
- Kleipool QL, Dobber MR, de Haan JF, and Levelt PF (2008), Earth surface reflectance climatology from 3 years of omi data, *Journal of Geophysical Research: Atmospheres*, 113(D18), doi:10.1029/2008JD010290.
- Kramer LJ, Leigh RJ, Remedios JJ, and Monks PS (2008), Comparison of OMI and ground-based in situ and MAX-DOAS measurements of tropospheric nitrogen dioxide in an urban area, *Journal of Geophysical Research: Atmospheres*, 113(D16), doi: 10.1029/2007JD009168.
- Krotkov NA, McLinden CA, Li C, Lamsal LN, Celarier EA, Marchenko SV, Swartz WH, Bucsela EJ, Joiner J, Duncan BN, Boersma KF, Veefkind JP, Levelt PF, Fioletov VE, Dickerson RR, He H, Lu Z, and Streets DG (2016), Aura OMI observations of regional SO₂ and NO₂ pollution changes from 2005 to 2015, *Atmospheric Chemistry and Physics*, 16(7), 4605–4629, doi:10.5194/acp-16-4605-2016.
- Krotkov NA, Lamsal LN, Celarier EA, Swartz WH, Marchenko SV, Bucsela EJ, Chan KL, Wenig M, and Zara M. (2017), The version 3 omi no₂ standard product, *Atmospheric Measurement Techniques*, 10(9), 3133–3149, doi:10.5194/amt-10-3133-2017.
- Levelt PF, van den Oord GHJ, Dobber MR, Mälkki A, Visser H, de Vries J, Stammes P, Lundell JOV, and Saari H. (2006), The Ozone Monitoring Instrument, *IEEE Trans. Geosci. Remote Sens*, 44, 1093.
- Lorente A, Folkert Boersma K, Yu H, Dörner S, Hilboll A, Richter A, Liu M, Lamsal LN, Barkley M, De Smedt I, Van Roozendaal M, Wang Y, Wagner T, Beirle S, Lin J-T, Krotkov N, Stammes P, Wang P, Eskes HJ, and Krol M. (2017), Structural uncertainty in air mass factor calculation for

- NO₂ and HCHO satellite retrievals, *Atmospheric Measurement Techniques*, 10(3), 759–782, doi:10.5194/amt-10-759-2017.
- Lu Z, and Streets DG (2012), Increase in NO_x emissions from Indian thermal power plants during 1996–2010: Unit-based inventories and multisatellite observations, *Environmental Science & Technology*, 46(14), 7463–7470, doi:10.1021/es300831w. [PubMed: 22732062]
- Marchenko S, Krotkov NA, Lamsal LN, Celarier EA, Swartz WH, and Bucsela EJ (2015), Revising the slant column density retrieval of nitrogen dioxide observed by the ozone monitoring instrument, *Journal of Geophysical Research: Atmospheres*, 120(11), 5670–5692, doi:10.1002/2014JD022913.
- McLinden CA, Fioletov V, Boersma KF, Krotkov N, Sioris CE, Veefkind JP, and Yang K. (2012), Air quality over the Canadian oil sands: A first assessment using satellite observations, *Geophysical Research Letters*, 39(4), doi:10.1029/2011GL050273.
- McLinden CA, Fioletov V, Boersma KF, Kharol SK, Krotkov N, Lamsal L, Makar PA, Martin RV, Veefkind JP, and Yang K. (2014), Improved satellite retrievals of NO₂ and SO₂ over the Canadian oil sands and comparisons with surface measurements, *Atmospheric Chemistry and Physics*, 14(7), 3637–3656, doi:10.5194/acp-14-3637-2014.
- McLinden CA, Fioletov V, Krotkov NA, Li C, Boersma KF, and Adams C. (2016), A Decade of Change in NO₂ and SO₂ over the Canadian Oil Sands As Seen from Space, *Environmental Science & Technology*, 50(1), 331–337, doi: 10.1021/acs.est.5b04985. [PubMed: 26642237]
- Noxon JF (1975), Nitrogen dioxide in the stratosphere and troposphere measured by ground-based absorption spectroscopy, *Science*, 189(4202), 547–549, doi: 10.1126/science.189.4202.547. [PubMed: 17798301]
- O’Byrne G, Martin RV, van Donkelaar A, Joiner J, and Celarier EA (2010), Surface reflectivity from the Ozone Monitoring Instrument using the Moderate Resolution Imaging Spectroradiometer to eliminate clouds: Effects of snow on ultraviolet and visible trace gas retrievals, *Journal of Geophysical Research: Atmospheres*, 115(D17), doi: 10.1029/2009JD013079.
- Palmer PI, Jacob DJ, Chance K, Martin RV, Spurr RJD, Kurosu TP, Bey I, Yantosca R, Fiore A, and Li Q. (2001), Air mass factor formulation for spectroscopic measurements from satellites: Application to formaldehyde retrievals from the Global Ozone Monitoring Experiment, *Journal of Geophysical Research: Atmospheres*, 106(D13), 14,539–14,550, doi:10.1029/2000JD900772.
- Percy KE, Hansen MC, and Dann T. (2012), Air Quality in the Athabasca Oil Sands Region, in Volume 11: Alberta Oil Sands - Energy, Industry and the Environment, 1 ed., Elsevier.
- Platt U, and Stutz J. (2008), *Differential Optical Absorption Spectroscopy: Principles and Applications*, Springer, Berlin, Germany.
- van Geffen JHGM, Boersma KF, Van Roozendaal M, Hendrick F, Mahieu E, De Smedt I, Snee M, and Veefkind JP (2015), Improved spectral fitting of nitrogen dioxide from OMI in the 405–465 nm window, *Atmospheric Measurement Techniques*, 8(4), 1685–1699, doi:10.5194/amt-8-1685-2015.
- van Geffen JHGM, Eskes HJ, Boersma KF, Maasackers JD, and Veefkind JP (2018), TROPOMI ATBD of the total and tropospheric NO₂ data products, issue 1.2.0 ed., s5P-KNMI-L2–0005-RP.
- Veefkind J, Aben I, McMullan K, Forster H, de Vries J, Otter G, Claas J, Eskes H, de Haan J, Kleipool Q, van Weele M, Hasekamp O, Hoogeveen R, Landgraf J, Snel R, Tol P, Ingmann P, Voors R, Kruizinga B, Vink R, Visser H, and Levelt P. (2012), TROPOMI on the ESA Sentinel-5 Precursor: A GMES mission for global observations of the atmospheric composition for climate, air quality and ozone layer applications, *Remote Sensing of Environment*, 120, 70 – 83, doi: 10.1016/j.rse.2011.09.027, the Sentinel Missions - New Opportunities for Science.
- Williams JE, Boersma KF, Le Sager P, and Verstraeten WW (2017), The high-resolution version of TM5-MP for optimized satellite retrievals: description and validation, *Geoscientific Model Development*, 10(2), 721–750, doi:10.5194/gmd-10-721-2017.
- Zara M, Boersma KF, De Smedt I, Richter A, Peters E, van Geffen JHGM, Beirle S, Wagner T, Van Roozendaal M, Marchenko S, Lamsal LN, and Eskes HJ (2018), Improved slant column density retrieval of nitrogen dioxide and formaldehyde for omi and gome-2a from qa4ecv: intercomparison, uncertainty characterisation, and trends, *Atmospheric Measurement Techniques*, 11(7), 4033–4058, doi:10.5194/amt-11-4033-2018.

Zawada DJ, Dueck SR, Rieger LA, Bourassa AE, Lloyd ND, and Degenstein DA (2015), High-resolution and monte carlo additions to the sasktran radiative transfer model, *Atmospheric Measurement Techniques*, 8(6), 2609–2623, doi:10.5194/amt-8-2609-2015.

NASA Author Manuscript

NASA Author Manuscript

NASA Author Manuscript

Key Points:

- First evaluation of the TROPOMI NO₂ retrieval product
- The quality of the TROPOMI NO₂ data is unprecedented and captures variation on a very high spatial resolution
- TROPOMI tropospheric NO₂ retrievals can be corrected with higher resolution input data

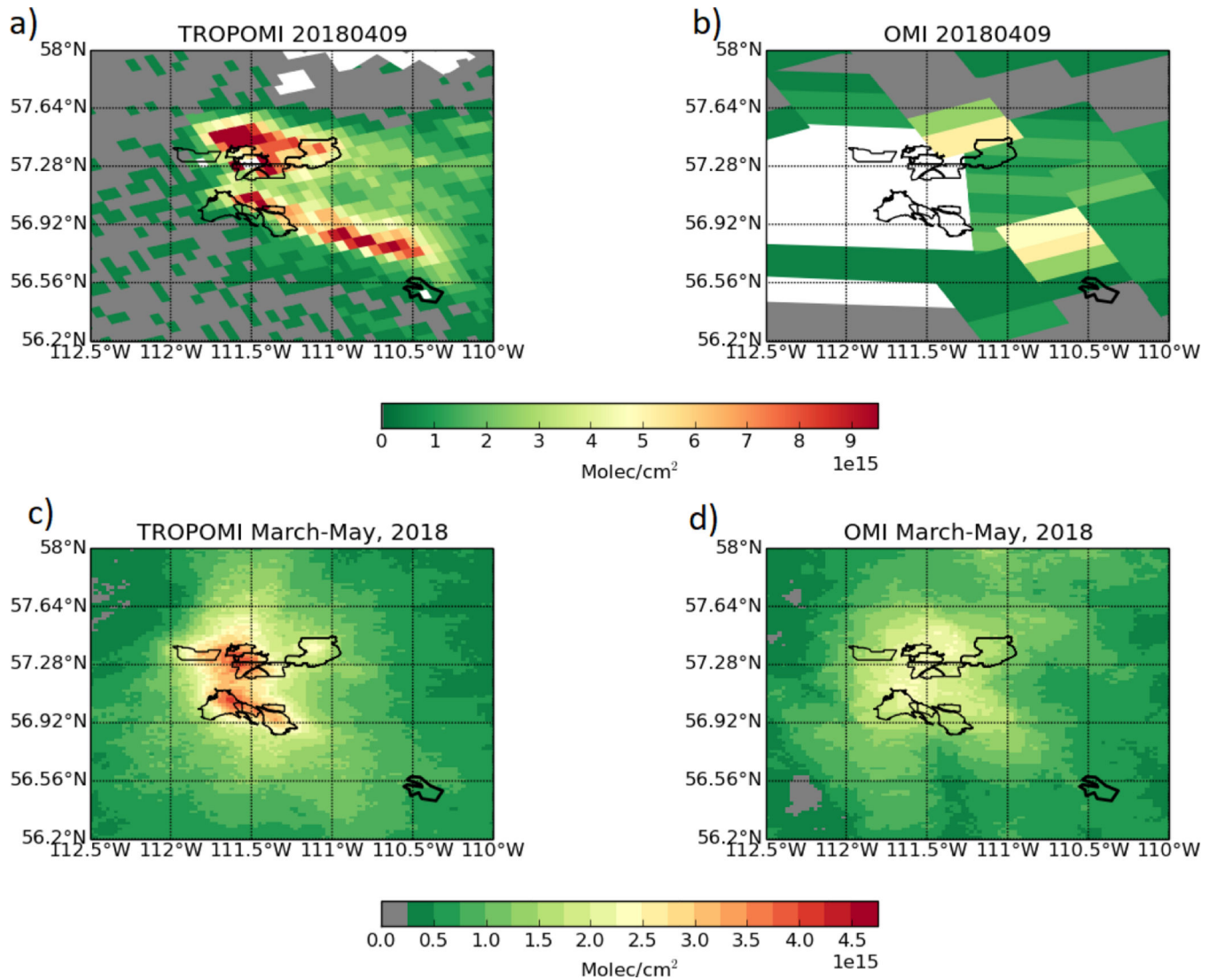


Figure 1. NO₂ measured by TROPOMI (a) and OMI (b) on April 9, 2018 over the surface mines of the AOSR (with NW winds). Averages (March-May, 2018) with an averaging radius of 5 km and 16 km was used for TROPOMI (c) and OMI (d), respectively. The black line traces the borders of the individual mining operations.

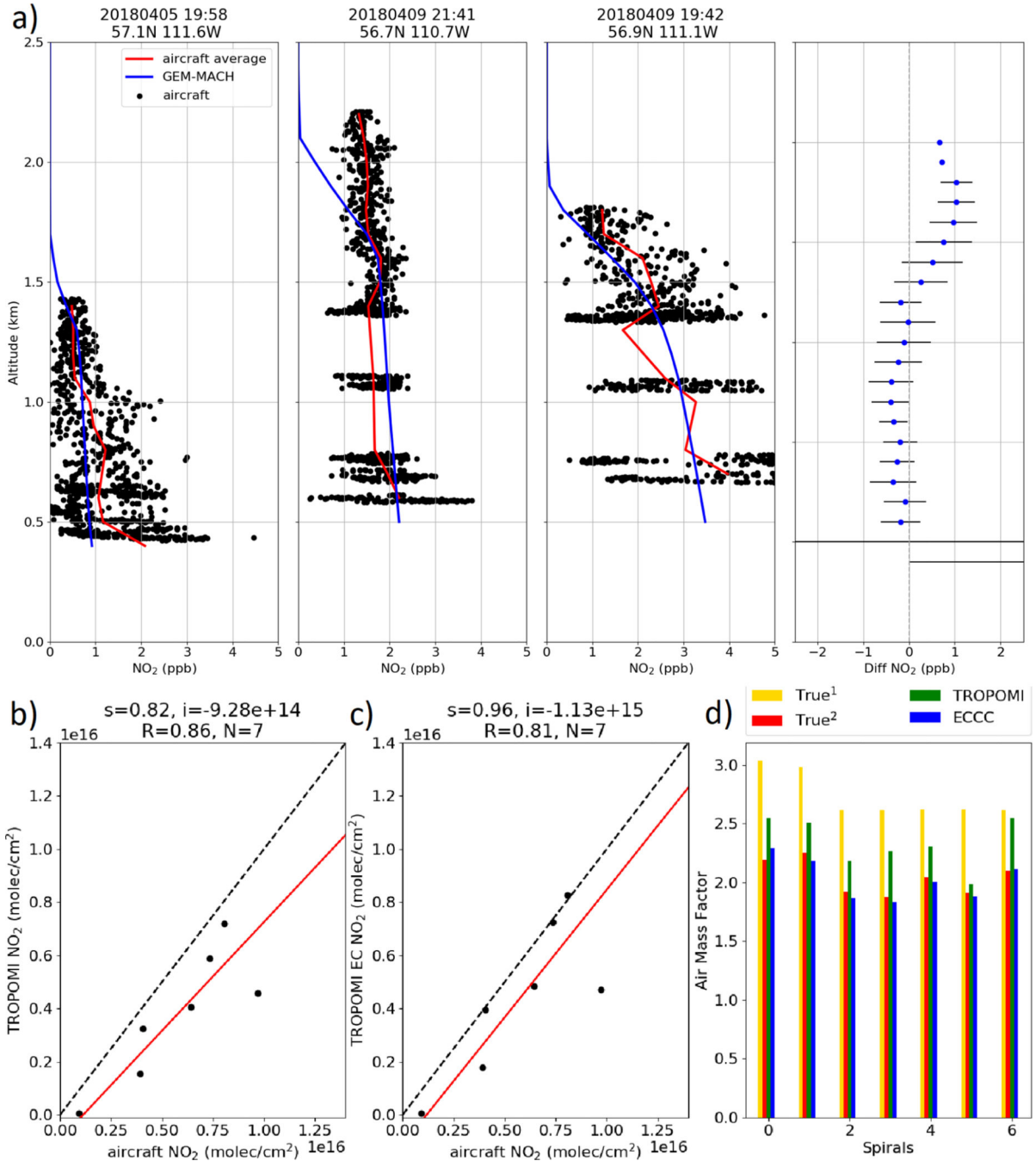


Figure 2.

(a) In-situ aircraft measurements and GEM-MACH model output of the three of the seven spiral flights that are within retrieved TROPOMI pixels. The right figure shows the mean difference (and standard deviation) between the GEM-MACH model and the aircraft measurements from all seven spirals. Aircraft columns versus (b) the original and (c) the alternative AMF TROPOMI NO₂ columns. The solid red and the black dashed lines represent the line of best fit and the 1:1 line, respectively. (d) AMFs, including the original TROPOMI (AMF TROPOMI; green), the re-calculated (AMF EC; blue), and the calculated

“true” AMF from aircraft measurements using the TROPOMI albedo (True 1; yellow) the MODIS albedo (True 2; red).

NASA Author Manuscript

NASA Author Manuscript

NASA Author Manuscript

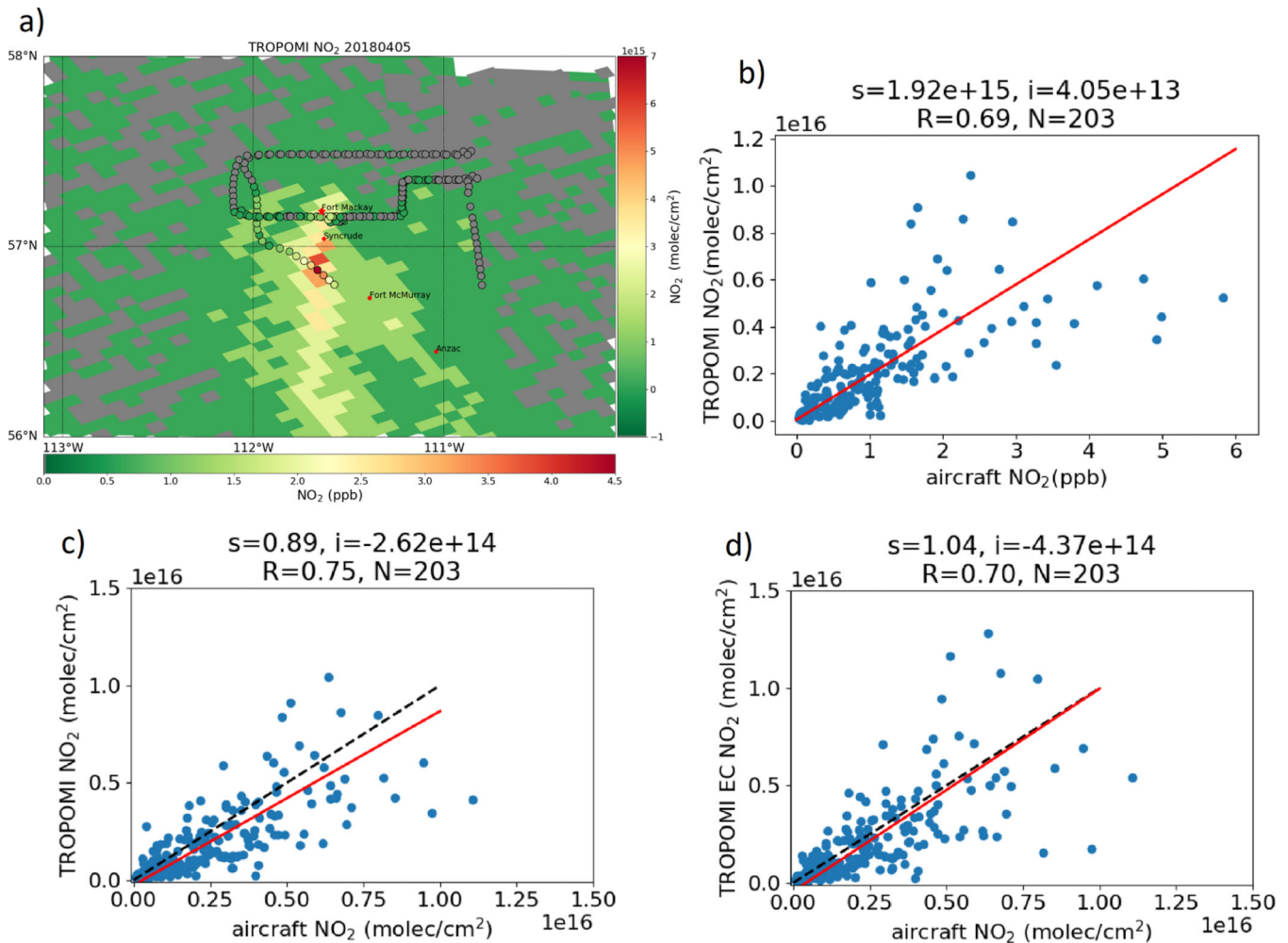


Figure 3.

(a) Map around the AOSR showing the NO₂ VMRs as sampled by the aircraft (for clarity of the plot the averages of 30 data points are shown) and TROPOMI tropospheric NO₂ VCD pixels for April 5, 2018. TROPOMI tropospheric NO₂ columns versus aircraft in-situ measurements (b), the aircraft “VCDs” (Eq. 1) (c), and the aircraft “VCDs” versus the alternative TROPOMI columns (d). For the regression analysis, we use a geometric mean analysis with $y = sx + i$ (s and i values are indicated in the plots, as well as the correlation coefficient, R and the number of points, N).

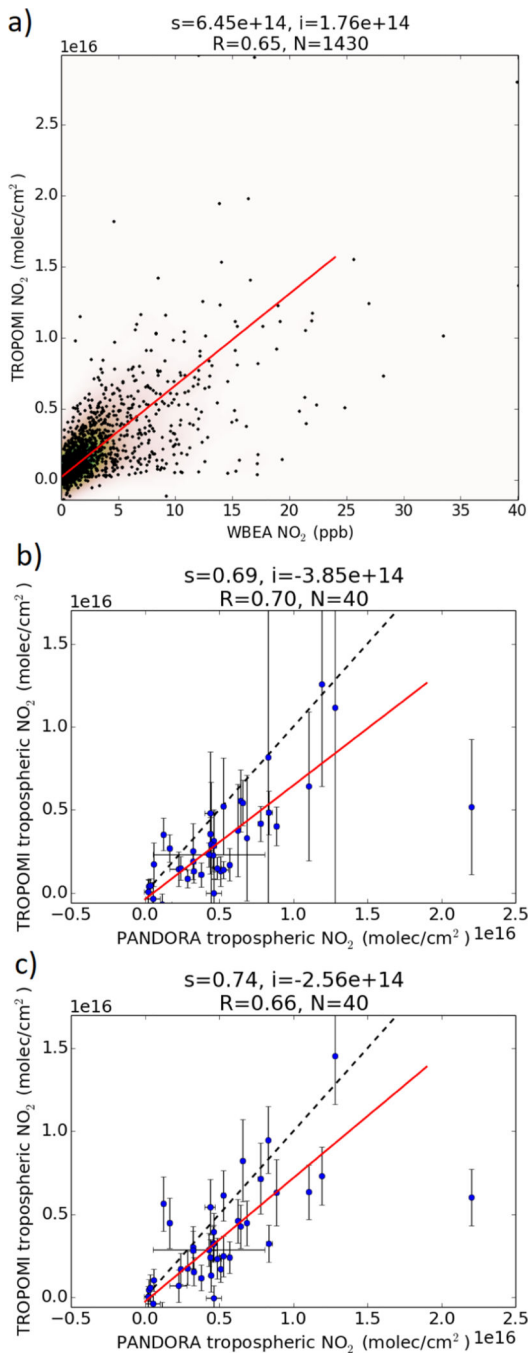


Figure 4. TROPOMI tropospheric NO_2 columns versus the ground-based in-situ (a) and remote-sensing Pandora measurements (b-c) for: (b) the original TROPOMI columns, and (c) the alternative columns.